

Model-based feed-forward control for time-varying systems with an example for SRF cavities

Sven Pfeiffer* Annika Eichler* Holger Schlarb*

* *Deutsches Elektronen Synchrotron, Notkestr. 85, 22607 Hamburg
(e-mail: {sven.pfeiffer, annika.eichler, holger.schlarb}@desy.de).*

Abstract: To derive feed-forward signals the impulse response matrix has to be inverted. While for time-invariant systems this matrix has a Toeplitz structure, this is not the case for time-variant systems. Thus, the derivation of the inverse scales cubically with the length of the signal horizon. This paper presents an efficient way to calculate the inverse impulse response matrix based on the description as linear fractional transformation. With this the calculation effort scales only linearly with the horizon. The feed-forward signal generation is applied in this paper for superconducting accelerating structures. The superconducting accelerating cavities are operated in pulsed mode. Each cavity is fed by a 1.3 GHz radio frequency signal with high power. Model-based feed-forward control is essential here to relief the feedback controller and with this to minimize the power consumption and therefore heating of different components. To derive a model-based feed-forward signal, first, a reasonable reference signal is to be chosen, which is done here based on physical properties of the cavities, then the efficient inversion of the impulse response matrix is applied. Experimentally results from the European X-ray free-electron laser are presented.

Keywords: Free-electron laser, RF superconducting cavity, feed-forward optimization, set-point optimization, model-based optimization, linear fractional transformation, impulse response matrix.

1. INTRODUCTION

The European X-ray free-electron laser (EuXFEL) is a user facility operated by the European XFEL GmbH. The main purpose is to generate X-ray laser flashes for chemical, biological, physical and other experiments, Altarelli et al. (2006). Hereby, electrons are accelerated in a burst mode to almost speed of light, forced on a sinusoidal trajectory emitting X-rays used for the experiments. The acceleration of the electrons is achieved by superconducting cavities with field gradient up to 30 MV/m. The cavity fields are active in a pulsed mode with 1% duty cycle in 10 Hz operation. The field gradients need to be regulated to precision of 0.01% in amplitude and 0.01 deg. in phase. A feed-forward drive and feedback loop is implemented in a low-level radio frequency (LLRF) controller. The high demands in RF field control are accomplished with feed-forward signal together with iterative learning control and a fast feedback loop implemented on a field programmable gate array (FPGA). The used feedback schemes are based on system models developed over the last years, Kirchhoff et al. (2008), Schmidt et al. (2008), Pfeiffer et al. (2012).

Feed-forward control is an essential task to setup an RF station at the EuXFEL. The derivation of an optimized feed-forward signal in open loop has been discussed in Ayvazyan et al. (2010). This optimized signal generation scheme, which is currently used by manual tuning, is based on a system model taking only one cavity parameter into account, i.e., the half-bandwidth, while the detuning

which is a time-varying effect is neglected. In this work the detuning is considered for feed-forward generation and it is not restricted to feed-forward only which allows for direct closed-loop optimization without changing operational conditions.

We describe the cavity system in lifted representation to invert the system response for the computation of the optimal feed-forward signal. In the lifted system representation, a static map representing the convolution, is used to describe the system dynamics. Commonly, a convolution matrix (or impulse response matrix) with finite dimensions is used to describe linear systems, e.g., in iterative learning control by Dijkstra and Bosgra (2003). In Lunenburg (2009), it is shown how the lifted system representation for linear systems can be used for feed-forward control design. Their proposed method is relatively straightforward: the impulse response matrix used in the lifted system representation is inverted and the resulting matrix can be used to compute the feed-forward signal. Note that for time-invariant the impulse response matrix is a Toeplitz matrix, which is not the case for time-varying systems. In case of a minimum phase system, this leads to the exact tracking of an arbitrary reference trajectory. Due to the high data rate as in the application of SRF cavities with a sampling frequency of 9 MHz, this lifted representation and especially the inversion of impulse response matrix is time consuming, since it scales cubically with the time horizon, Boyd and Vandenberghe (2004). Therefore, an alternative method for inversion based on the representation as linear fractional transformation is developed here to

deal with the high computational effort. Exploiting the inversion properties of linear fractional transformations the derivation of the inverse impulse response matrix scales only linearly with the time horizon.

The paper is organized as follows: Section 2 focuses on the theoretical approach of the inversion of the impulse response for time-varying systems. The application of the results at the EuXFEL is presented in the next two sections. First, in Section 3 an introduction to the considered system is given, followed by the feed-forward optimization shown in Section 4 using the theoretic results from Section 2. Section 5 concludes the paper.

2. INVERSION OF IMPULSE RESPONSE MATRIX

Given any causal time-varying discrete-time system

$$\begin{aligned} x_{k+1} &= A_k x_k + B_k u_k, \\ y_k &= C_k x_k. \end{aligned} \quad (1)$$

The vectors $x_k \in \mathbb{R}^n$, $u_k \in \mathbb{R}^m$ and $y_k \in \mathbb{R}^l$ concatenate the system states, inputs and outputs at time k . The system matrices $A_k = A(k)$, $B_k = B(k)$ and $C_k = C(k)$ are real matrices, which are time-varying, i.e., they depend on time k . They are assumed to be known and of appropriate dimensions.

2.1 Impulse Response Matrix

The output of system (1) is given by the impulse response matrix (IRM)

$$y_{k+1} = C_{k+1} \left(B_k u_k + \sum_{i=0}^{k-1} \left(\prod_{j=i+1}^k A_j \right) B_i u_i \right) \quad (2)$$

or in lifted system representation, Lunenburg (2009), with time dependent parameters A_k, B_k and C_k as lower triangular matrix mapping the inputs to the outputs

$$[y]_1^{K+1} = H_{\text{IRM}} \cdot [u]_0^K,$$

with H_{IRM}

$$= \begin{bmatrix} C_1 B_0 & 0 & \vdots & 0 \\ C_2 A_1 B_0 & C_2 B_1 & \vdots & 0 \\ \vdots & \vdots & \ddots & \vdots \\ C_{K+1} \left(\prod_{l=1}^K A_l \right) B_0 & C_{K+1} \left(\prod_{l=2}^K A_l \right) B_1 & \vdots & C_{K+1} B_K \end{bmatrix}. \quad (3)$$

The input $[u]_0^K$ and output $[y]_1^{K+1}$ are the stacked vectors for the times $k = 0, 1, \dots, K$ ($k = 1, \dots, K + 1$, respectively) given by

$$\begin{aligned} [u]_0^K &= [u_0^\top \ u_1^\top \ \dots \ u_K^\top]^\top \text{ and} \\ [y]_1^{K+1} &= [y_1^\top \ y_2^\top \ \dots \ y_{K+1}^\top]^\top, \text{ respectively.} \end{aligned}$$

This impulse matrix differs from its linear time-invariant counterpart which is given as Toeplitz matrix. It is not a pure Toeplitz matrix anymore for such time-varying system characteristics, but the structure stays the same.

In the following we assume (without loss of generality) that the system is neither underactuated nor overactuated, i.e., the number of inputs m equals the number of outputs l .

2.2 Inverse Impulse Response Matrix

To calculate the input $[u]_0^K$ for a desired reference trajectory, we need to invert the IRM as

$$[u]_0^K = H_{\text{IRM}}^{-1} \cdot [y]_1^{K+1}. \quad (4)$$

The IRM is a $(K + 1)m \times (K + 1)m$ dimensional matrix. Deriving the matrix itself requires $(K + 1)(2mn^2 - mn) + \sum_{i=1}^K (2mn^2 - mn + 2m^2n - m^2) = (K + 1)(2mn^2 - mn) + \frac{K(K+1)}{2}(2mn^2 - mn + 2m^2n - m^2)$ floating point operations (FLOPs); the basic terms for FLOP calculations are given as supplementary information in Sec. 6. Note that here it is considered that the term $\prod_{j=1}^i A_j$, which is needed in the i -th lower block diagonal, can be reused to calculate the respective term in the $i + 1$ -th lower block diagonal. To derive the inverse $(Km + m)^3$ FLOPs are required additionally, leading to a total of

$$o_{\text{direct}} = (Km + m)^3 + (K + 1)(2mn^2 - mn) + \frac{K(K + 1)}{2}(2mn^2 - mn + 2m^2n - m^2). \quad (5)$$

This might be computational challenging for large K and fast applications like the one considered in Section 3. Therefore, the goal is to simplify the calculation. To do so, we use the concept of linear fractional transformations (LFTs). An introduction of this concept is given in Doyle et al. (1991) and the concepts used in this paper are briefly reviewed here.

Given a complex matrix M partitioned as

$$M = \begin{bmatrix} M_{11} & M_{12} \\ M_{21} & M_{22} \end{bmatrix} \in \mathbb{C}^{(p_1+p_2) \times (q_1+q_2)}$$

and let $D_2 \subset \mathbb{C}^{p_2 \times q_2}$, then a (lower) linear fractional transformation maps $F_l(M, \bullet) : D_2 \mapsto \mathbb{C}^{p_1 \times q_1}$ with

$$F_l(M, \Delta_l) := M_{11} + M_{12} \Delta_l (I - M_{22} \Delta_l)^{-1} M_{21}.$$

A graphical representation of the lower LFT as block diagram is shown in Fig. 1.

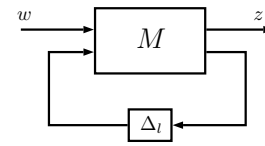


Fig. 1. Lower LFT connection.

Rewriting H_{IRM} as LFT leads to

$$H_{\text{IRM}} := M_{11} + M_{12} \Delta_l (I - M_{22} \Delta_l)^{-1} M_{21}, \quad (6)$$

with

$$\begin{aligned} \Delta_l &= \begin{bmatrix} A_1 & & & \\ & A_2 & & \\ & & \ddots & \\ & & & A_k \end{bmatrix} \in \mathbb{R}^{Kn \times Kn}, \\ M_{11} &= \begin{bmatrix} C_1 B_0 & & & \\ & C_2 B_1 & & \\ & & \ddots & \\ & & & C_{K+1} B_K \end{bmatrix} \in \mathbb{R}^{(K+1)m \times (K+1)m}, \end{aligned}$$

$$M_{12} = \begin{bmatrix} 0 & 0 & \dots & 0 & 0 \\ C_2 & 0 & \dots & 0 & 0 \\ 0 & C_3 & \dots & 0 & 0 \\ \vdots & & & \ddots & \vdots \\ 0 & 0 & \dots & 0 & C_{K+1} \end{bmatrix} \in \mathbb{R}^{(K+1)m \times Kn},$$

$$M_{21} = \begin{bmatrix} B_0 & 0 & \dots & 0 & 0 & 0 \\ 0 & B_1 & \dots & 0 & 0 & 0 \\ \vdots & & & \ddots & \vdots & \\ 0 & 0 & \dots & B_{K-1} & 0 & 0 \end{bmatrix} \in \mathbb{R}^{Kn \times (K+1)m} \text{ and}$$

$$M_{22} = \begin{bmatrix} 0 & 0 & \dots & 0 & 0 \\ I & 0 & \dots & 0 & 0 \\ \vdots & & & \ddots & \vdots \\ 0 & 0 & \dots & I & 0 \end{bmatrix} \in \mathbb{R}^{Kn \times Kn}.$$

Except of M_{11} , requiring $(K+1)(2m^2n - m^2)$ FLOPs, these matrices do not need any calculations.

We can make use of the properties for LFTs given in Doyle et al. (1991) to calculate the inverse, which is given by $F_l(M, \Delta)^{-1} = F_l(\hat{M}, \Delta)$ with

$$\hat{M} = \begin{bmatrix} M_{11}^{-1} & -M_{11}^{-1}M_{12} \\ M_{21}M_{11}^{-1} & M_{22} - M_{21}M_{11}^{-1}M_{12} \end{bmatrix} = \begin{bmatrix} \hat{M}_{11} & \hat{M}_{12} \\ \hat{M}_{21} & \hat{M}_{22} \end{bmatrix}. \quad (7)$$

In \hat{M} the inverse of M_{11} appears, which is the calculated by inverting the block-diagonal elements. Thus, calculating M_{11}^{-1} requires $(K+1)(\frac{8}{3}m^3 + 2m^2n - m^2)$ FLOPs.

In the following we will distinguish two cases

- I: B (and thus also C) are squared, i.e., $n = m$.
- II: B is not squared, i.e., $n > m$.

Case I: $n = m$ The lower right block of \hat{M} , \hat{M}_{22} , simplifies to zero. Thus,

$$H_{\text{IRM}}^{-1} = F_l(M, \Delta)^{-1} = F_l(\hat{M}, \Delta)$$

$$= \hat{M}_{11} + \hat{M}_{12}\Delta_l(I - \hat{M}_{22}\Delta_l)^{-1}\hat{M}_{21}$$

$$= \hat{M}_{11} + \hat{M}_{12}\Delta_l\hat{M}_{21}$$

$$= \begin{bmatrix} (C_1B_0)^{-1} & 0 & \dots & 0 & 0 \\ -B_1^{-1}A_1C_1^{-1} & (C_2B_1)^{-1} & \dots & 0 & 0 \\ 0 & -B_2^{-1}A_2C_2^{-1} & \ddots & 0 & \vdots \\ \vdots & \vdots & \ddots & \ddots & 0 \\ 0 & 0 & \dots & -B_K^{-1}A_KC_K^{-1} & (C_{K+1}B_K)^{-1} \end{bmatrix}. \quad (8)$$

To calculate $\hat{M}_{12}\Delta_l\hat{M}_{21}$ it requires $K(\frac{28}{3}n^3 - 2n^2)$ FLOPs. Thus, in total calculating $F_l(M, \Delta)^{-1}$ requires $o_{n=m}$ FLOPs with

$$o_{n=m} = (K+1)\left(\frac{14}{3}n^3 - n^2\right) + K\left(\frac{28}{3}n^3 - 2n^2\right). \quad (9)$$

Case II: $n > m$ The lower right block of \hat{M} , \hat{M}_{22} , does not simplify to zero, but to

$$\hat{M}_{22} = \begin{bmatrix} 0 & 0 & \dots & 0 & 0 & 0 \\ \hat{m}_{2,1} & 0 & \dots & 0 & 0 & 0 \\ 0 & \hat{m}_{3,2} & \dots & 0 & 0 & 0 \\ \vdots & & & \ddots & \vdots & 0 \\ 0 & 0 & \dots & 0 & \hat{m}_{K,K-1} & 0 \end{bmatrix},$$

with

$$\hat{m}_{i+1,i} = I - B_i(C_{i+1}B_i)^{-1}C_{i+1} \quad \text{for } i = 1, \dots, K-1.$$

Thus, the matrix $\Xi = I - \hat{M}_{22}\Delta_l$, which needs to be inverted in (7), is not a full lower triangular matrix but only the first off-diagonal blocks are full and the diagonal blocks are identity. With this the inverse Ξ^{-1} is

$$\Xi^{-1} = \begin{bmatrix} I & 0 & \dots & 0 & 0 & 0 \\ \hat{m}_{2,1}A_1 & I & \dots & 0 & 0 & 0 \\ 0 & \hat{m}_{3,2}A_2 & \dots & 0 & 0 & 0 \\ \vdots & & & \ddots & \vdots & 0 \\ 0 & 0 & \dots & 0 & \hat{m}_{K,K-1}A_{K-1} & I \end{bmatrix}.$$

To calculate the $(i, i-1)$ -th block entry of Ξ it requires $2m^2n + 2mn^2 - mn + 2n^3 - n^2$ FLOPs, but the inversion does not need any extra ones. Finally, the inverse of the impulse response matrix is given by

$$H_{\text{IRM}}^{-1} = \begin{bmatrix} f_{1,1} & 0 & 0 & \dots & 0 \\ f_{2,1} & f_{2,2} & 0 & \dots & 0 \\ f_{3,1} & f_{3,2} & f_{3,3} & \ddots & \vdots \\ 0 & \ddots & \ddots & \ddots & 0 \\ 0 & \dots & f_{K+1,K-1} & f_{K+1,K} & f_{K+1,K+1} \end{bmatrix}, \quad (10)$$

with

$$f_{i,i} = (C_iB_{i-1})^{-1} \quad \text{for } i = 1, \dots, K+1,$$

$$f_{i+1,i} = -(C_{i+1}B_i)^{-1}C_{i+1}A_iB_{i-1}(C_iB_{i-1})^{-1}$$

$$\quad \text{for } i = 1, \dots, K,$$

$$f_{i+2,i} = -(C_{i+2}B_{i+1})^{-1}C_{i+2}A_{i+1}\hat{m}_{i+1,i}A_iB_{i-1}(C_iB_{i-1})^{-1}$$

$$\quad \text{for } i = 1, \dots, K-1$$

and the total number of FLOPs, $o_{n>m}$, to calculate (10) is given by

$$o_{n>m} = (K+1)\left(2m^2n - m^2 + \frac{8}{3}m^3\right)$$

$$+ (K-1)(4m^2n - m^2 + 4mn^2 - 2mn + 2n^3 - n^2)$$

$$+ K(-mn + 4m^2n - m^2). \quad (11)$$

Here, it made use of the fact that the same multiplications do not need to be performed twice.

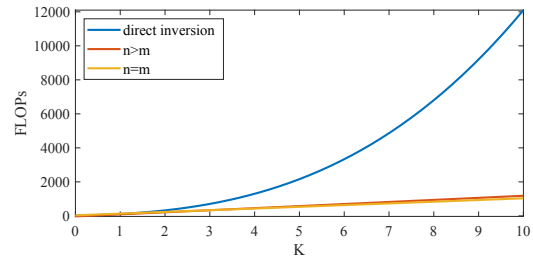


Fig. 2. Comparison of the number of FLOPs depending on K for an example case with $n = m = 2$.

Comparison Comparing (5), (9) and (11) shows that while the calculation and direct inversion of H_{IRM} as given in (3) is dominated by K^3 , when exploiting the LFT description leads to expressions of H_{IRM}^{-1} given in (8) or (10), which scale linearly with K .

For an example case of $n = m = 2$ this dependency of the number of FLOPs is shown in Fig. 2.

3. LLRF SYSTEM

The EuXFEL is operated in pulsed mode with an RF pulse length of about 1 ms. The typical filling and flattop operation is shown as example for one superconducting radio frequency (SRF) cavity in Fig. 3.

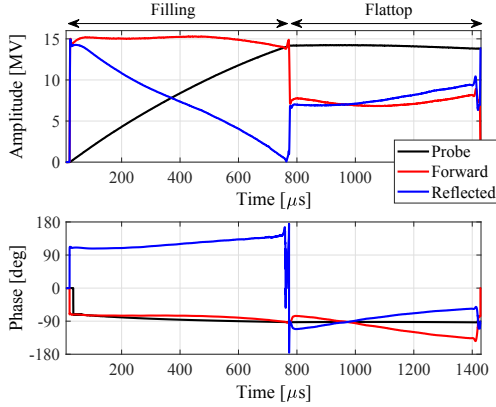


Fig. 3. Example of typical cavity probe, forward and reflected signals in baseband for filling and flattop phase.

During filling, the cavity is ramped to its nominal operating gradient in amplitude and phase. This probe amplitude and phase is kept as constant as possible during flattop while electrons are injected and accelerated. It is important to mention that the amplitude of a single cavity might not be perfectly flat during the flattop because of a vector-sum regulation scheme¹, Omet et al. (2018).

The vector-sum of each RF station is controlled by an LLRF system in closed-loop with a MIMO feedback controller and an iterative learning scheme. To relieve both of them, additional feed-forward control is essential. In this section a model for the LLRF system is derived such that the model-based feed-forward generation using the inversion of the impulse response matrix from the previous section can be applied. A block diagram of the RF system with the signal flow within it is shown in Fig. 4. The main

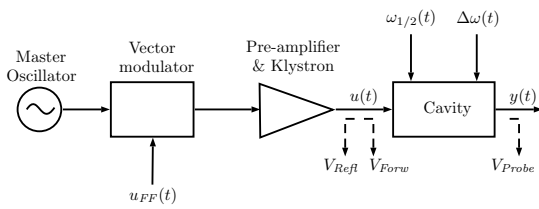


Fig. 4. RF station signal flow from low power LLRF drive $u_{FF}(t)$ via high power amplifiers to the cavity.

reference is the master oscillator (MO) providing a 1.3 GHz signal which is modulated by the vector modulator in amplitude and phase using the drive input $u_{FF}(t)$ from the control system. A pre-amplifier and klystron amplifies the

¹ The concept of the vector-sum regulation is particularly for the EuXFEL, since here due to the vast number of SRF cavities (776) not every cavity is driven by an individually high power amplifier and therefore controlled individually. Instead 32 cavities in one RF station are driven by one high power amplifier and controlled with respect to a common output, which is the so-called vector-sum, i.e., the sum of the outputs of the 32 cavities.

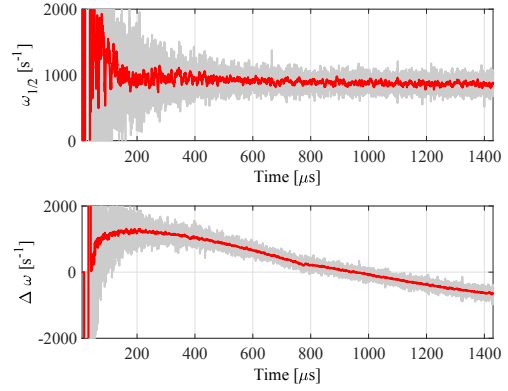


Fig. 5. Example of the half-bandwidth and detuning variation along an RF pulse.

RF signal from watt to megawatts which is then driving up to 32 cavities. For each cavity a forward, reflected and probe signal is detected with respect to the master oscillator and down-converted into baseband.

In the following we will first introduce the dynamic model of the cavity followed by a combined one for vector modulator, pre-amplifier and klystron, which can be represented as nonlinear static map.

3.1 Cavity model

The transfer function of a cavity in continuous time can be described in baseband, Schilcher (1998), by a first order transfer function in the complex plane

$$\frac{dV_{Probe}}{dt} = A_c(t) \cdot \underbrace{V_{Probe}}_{y(t)} + B_c(t) \cdot \underbrace{V_{Forw}}_{u(t)},$$

$$y(t) = C_c \cdot V_{Probe},$$

with system matrix $A_c(t)$ depending on the time-varying half-bandwidth $\omega_{1/2}(t)$ and the detuning $\Delta\omega(t)$ given as $A_c(t) = -\omega_{1/2}(t) + j \cdot \Delta\omega(t)$, the input matrix which is dependent on the half-bandwidth $B_c(t) = 2 \cdot \omega_{1/2}(t)$ and the output matrix $C_c = 1$. The system output $y(t)$ is given as complex cavity voltage $V_{Probe} \in \mathbb{C}$ and the input signal $u(t)$ is the complex forward voltage $V_{Forw} \in \mathbb{C}$.

In addition to the complex forward voltage and complex probe signal, the complex reflected voltage $V_{Refl} \in \mathbb{C}$ is measured, for which the relation $V_{Probe} = V_{Forw} + V_{Refl}$ holds. Drifts of the signals caused by temperature or humidity changes require a frequent calibration of the forward and reflected signal to the probe signal, Pfeiffer et al. (2015). With a proper signal calibration, the time-varying detuning $\Delta\omega(t)$ and the half-bandwidth $\omega_{1/2}$ can be determined. Example trajectories are shown in Fig. 3 and Fig. 5. These parameters, half-bandwidth and detuning, are additionally used for system health checks and further diagnostic and adaptation schemes, Rybaniec et al. (2014); Nawaz et al. (2016).

The transfer function in discrete time is given as

$$\begin{aligned} x_{k+1} &= A_{d,k}x_k + B_{d,k}u_k, \\ y_k &= C_d x_k, \end{aligned} \quad (12)$$

with time-varying discrete-time state matrix $A_{d,k}$, input matrix $B_{d,k}$ and output matrix C_d for sampling time

$T_s = 1/f_s$ and sampling frequency $f_s = 9$ MHz. To avoid discretization errors we make use of the exact discretization, i.e., the exact solution to the differential equation, giving the system matrices

$$\begin{aligned} A_d(k) &= e^{A_c(kT_s) \cdot T_s}, \\ B_d(k) &= A_c(kT_s)^{-1} \cdot (A_d(k) - I) \cdot B_c(kT_s) \text{ and} \\ C_d &= C_c. \end{aligned} \quad (13)$$

These time-varying matrices are valid only under the verified assumption that the bandwidth of detuning and half-bandwidth are small compared to the sampling frequency. Thus, the signals can be assumed to be constant within a sampling period. With these matrices, where the system matrix $A_{d,k} = A_d(k)$ and the input matrix $B_{d,k} = B_d(k)$ are time varying along the RF pulse, the impulse response matrix H_{IRM} in (3) for one pulse can be generated, resulting in $K = 12730$ for the given sampling frequency.

3.2 Vector modulator, pre-amplifier and klystron model

The vector modulator, modulating the baseband signals to RF, has linear input-output behavior, while the characteristic input-output behavior of the pre-amplifier and klystron is often nonlinear. It has been shown that the latter's output amplitude and phase is dependent on the input amplitude, Butkowski et al. (2016). The half-bandwidth of these components exceeds the range of 10 MHz such that we can assume a static input-output characteristic for the sampling frequency of 9 MHz. The dominating nonlinear effect that can be observed is the nonlinear amplitude dependence between the signal u_{FF} (input to the vector modulator) and the signal $V_{\text{Forw}} = u(t)$ (output of the klystron, which is the input to the cavity), while the non-linearity for the phase is up to a few degree neglectable. The nonlinear characteristic of the normalized amplitude is approximated with a static map using a polynomial of second order, see Fig. 6.

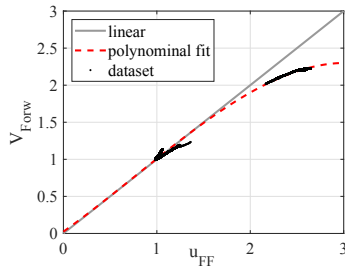


Fig. 6. Nonlinear characteristic between the LLRF drive signal u_{FF} and the input signal to the cavity V_{Forw} .

4. FEED-FORWARD OPTIMIZATION

To calculate an appropriate cavity forward signal, a desired reference signal (or set-point) is first formed. Then, the results in Section 2 can be applied to calculate the forward cavity input. Finally, the non-linearity of the pre-amplifier and klystron needs to be considered to calculate the LLRF feed-forward drive signal.

4.1 Reference signal generation

The reference signal is chosen with respect to the minimal power during filling, i.e. the most constant amplitude drive

signal and an on-resonance filling for a slightly detuned cavity during filling time. For the flattop the clear goal is to keep the voltage constant. The RF pulse is given by the two time periods filling and flattop:

- 1: Filling: $k_{\text{fill}} \in [1, \dots, \lceil t_{\text{fill}} \cdot f_s \rceil]$
- 2: Flattop: $k_{\text{flattop}} \in [k_{\text{fill}} + 1, \dots, \lceil t_{\text{flattop}} \cdot f_s \rceil]$

1: Filling The reference amplitude during filling is computed by the exponential filling using the averaged half-bandwidth (here $\bar{\omega}_{1/2} = 1000 \text{ s}^{-1}$) as

$$A_{SP}(k_{\text{fill}}) = K_{SP} \cdot (1 - \exp(-k_{\text{fill}}/f_s \cdot \bar{\omega}_{1/2})); \quad (14)$$

with K_{SP} as scaling factor to match the amplitude reference after filling. The mean detuning forms the phase reference by numerical integration with

$$\tilde{\phi}_{SP}(k_2) = - \sum_{k=1}^{k_2} \Delta f(k) \cdot 2\pi \quad (15)$$

for $k_2 = [1, \dots, k_{\text{fill}}]$. The detuning dependent phase reference is corrected using the nominal phase reference $\phi_{SP,static}$ and the last value of the detuning dependent phase $\tilde{\phi}_{SP}(k_{\text{fill},end})$ to

$$\phi_{SP} = \tilde{\phi}_{SP} - \tilde{\phi}_{SP}(k_{\text{fill},end}) + \phi_{SP,static}. \quad (16)$$

2: Flattop The reference signal during flattop is considered to be constant, i.e., equal to the static one. Remember, the amplitude and phase of the cavity RF field need to be regulated to be as constant as possible to achieve a constant acceleration of electrons for user experiments.

4.2 Feed-forward derivation

Given the reference signal derived in the previous part the forward signal for the cavities is derived using the inverse impulse response matrix for the model (12), matrices (13) and the maximum number of samples K given by the length of the reference signal, i.e., $K = 12730$ samples for filling and flattop for EuXFEL. With this, the number of FLOPs to calculate the inverse of the impulse response matrix directly as given in (5) is in the order of 10^{13} , while calculating the inverse of H_{IRM} based on the LFT description (8) is in the order of 10^6 . Note that for this example $n = m = 1$, thus case I can be considered. However, the formula for FLOPs given in (9) cannot be directly applied here, since it has been derived for real matrices, while the cavity system (12) is complex. System (12) can be equivalently described as two-dimensional symmetric real system with $n = m = 2$, see Schilcher (1998) leading to a slightly higher number of FLOPs. Since the calculation of FLOPs is general and does not exploit system symmetries, the exact number of FLOPs can be further reduced. The efficient implementation using (8) is further approved by the comparison of the calculation times for different values of K given in Table 1, where the linear dependency of (9) in contrast to the cubic dependency of (5) is confirmed.

The resulting forward signal for the cavity is corrected with the nonlinear map to derive the optimal LLRF feed-forward signal.

In Fig. 7 the closed-loop input signal to the cavities and the respective closed-loop output as vector-sum are

Table 1. Required time of computing the inverse system matrix using IRM (5) and LFT (9) with Matlab (1.6 GHz, 24 core, no parallel processing used)

| K | 256 | 512 | 1024 | 2048 | 4096 | 8192 |
|-----|--------|--------|--------|--------|-------|--------|
| IRM | 0.15 s | 0.7 s | 3.77 s | 21.4 s | 152 s | 1120 s |
| LFT | 5.6 ms | 5.7 ms | 7.4 ms | 15 ms | 26 ms | 60 ms |

shown for the reference signal used so far (old) and that described in Section 4.1 (new), designed for minimal power consumption. As mentioned above the outputs are not the outputs of a single cavity, but the vector-sum of the 32 cavities². The input signals include the feed-forward signals, the ILC and the feedback components, but the dominating effect is the feed-forward signal. Like this, as desired, ILC and the feedback-controller are relieved. Furthermore, with respect to the input it can be seen that with the reference signal derived in Section 4.1 compared to the one so far, the input peak power could be reduced.

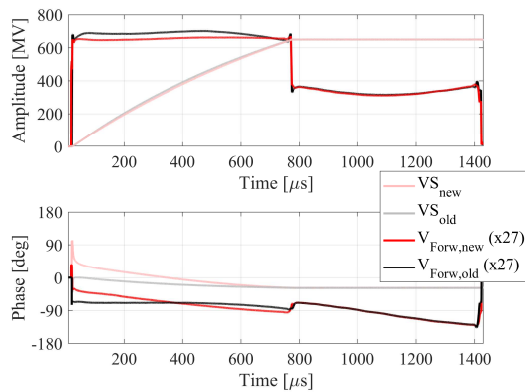


Fig. 7. Scaled controller drive signals and the corresponding vector-sum signals¹ for the reference signal used so far (old) and that described in Section 4.1 (new).

5. CONCLUSION

This contribution presents a feed-forward generation using the inverse impulse response matrix using linear fractional transformations. The advantage of the chosen approach is in computational reduction, which makes it highly suitable for fast adaptations of the reference and feed-forward signal with environmental changes such as detuning changes caused by reference changes. The efficiency of the approach is experimentally validated for the LLRF system at the EuXFEL.

REFERENCES

Altarelli, M. et al. (2006). XFEL, the European X-ray free-electron laser: Technical design report, DESY XFEL Project Group.
 Ayvazyan, V. et al. (2010). Optimization of Filling Procedure for TESLA-type Cavities for Klystron RF Power Minimization of European XFEL, in *Proc. 1st IPAC*, Kyoto, Japan.

² Every cavity has its own input-output characteristic while there is only one input signal feasible by the common drive. Therefore, the inverse of the impulse response matrix for each of the 32 cavities is calculated and added.

Boyd, S., and Vandenberghe, L. (2004). *Convex Optimization*, Cambridge University Press.
 Butkowski, L. et al. (2016). Model Based Fast Protection System for High Power RF Tube Amplifiers Used at European XFEL Accelerator, in *Proc. 20th IEEE-NPSS Real Time Conference*, Padua, Italy.
 Dijkstra, B.G., and Bosgra, O.H. (2003). Exploiting iterative learning control for input shaping, with application to a wafer stage, in *Proc. 2003 ACC*, Denver, USA.
 Doyle, J.C., Packard, A., and Zhou, K. (1991). Review of LFTs, LMIs and μ , in *Proc. 30th IEEE CDC*, Brighton, UK.
 Kirchoff, S. et al. (2008). An iterative learning algorithm for control of an accelerator based Free Electron Laser, in *Proc. 47th IEEE CDC*, Cancun, Mexico.
 Lunenburg, J.J.M. (2009). *Inversion-Based Feedforward Design for Beyond Rigid Body Systems: A Literature Survey*, DCT Report 2009.105, Eindhoven.
 Nawaz, A. et al. (2016). Self-Organized Critical Control for the European XFEL Using Black Box Parameter Identification for the Quench Detection System, in *Proc. 3rd Conference on Control and Fault-Tolerant Systems*, Barcelona, Spain.
 Omet, M. et al. (2018). LLRF Operation and Performance at the European XFEL, in *Proc. 9th IPAC*, Vancouver, Canada.
 Pfeiffer, S. et al. (2012). Design of an Optimal and Robust Controller for a Free-Electron Laser Exploiting Symmetries of the RF-System, in *Proc. 51th IEEE CDC*, Maui, HI, USA.
 Pfeiffer, S. et al. (2015). Virtual Cavity Probe Generation using Calibrated Forward and Reflected Signals, in *Proc. 6th IPAC*, Richmond, Virginia, USA.
 Rybaniec, R. et al. (2014). Real-time Estimation of Superconducting Cavities Parameters, in *Proc. 5th IPAC*, Dresden, Germany.
 Schilcher, T. (1998). Vector sum control of pulsed accelerating fields in Lorentz force detuned superconducting cavities, PhD thesis, Hamburg University.
 Schmidt, C. et al. (2008). Parameter estimation and tuning of a multivariable RF controller with FPGA technique for the Free Electron Laser FLASH, in *Proc. 2008 ACC*, Seattle, Washington, USA.

6. SUPPLEMENTARY MATERIAL

The floating point operations for matrix calculus as given in Boyd and Vandenberghe (2004), which are needed within the paper, are given for completeness.

- *Addition*: The addition $A + B$ of matrices $A, B \in \mathbb{R}^{m \times n}$ requires mn FLOPs.
- *Multiplication*: The multiplication AB of matrices $A \in \mathbb{R}^{m \times n}$ and $B \in \mathbb{R}^{n \times l}$ requires $2ml - ml$ FLOPs.
- *Inversion of a lower triangular matrix*: The inversion A^{-1} of a matrix lower triangular matrix $A \in \mathbb{R}^{n \times n}$ requires n^3 FLOPs, which results from solving the linear equation $Ax = e_i$ for n -times.
- *Inversion of a full matrix*: The inversion A^{-1} of a matrix $A \in \mathbb{R}^{n \times n}$ requires $\frac{8}{3}n^3$ FLOPs using LU-factorization.

For a specific problem the number of FLOPs for inversion can be further reduced by an appropriate factorization.